Hybrid photoiniferter and ring-opening polymerization yields one-pot anisotropic nanorods

Paul Joshua Hurst,[1] Junsik Yoon,[1] Riya Singh,[1] Mohammed Faris Abouchaleh,[1] Kevin A. Stewart,[2] Brent S. Sumerlin,[2] Joseph P. Patterson.*[1,3]

Affiliations
1. Department of Chemistry, University of California, Irvine, Irvine, CA, 92697, United States
2. George & Josephine Butler Polymer Research Laboratory, Center for Macromolecular Science & Engineering, Department of Chemistry, University of Florida, Gainesville, FL, 32611, United States
3. Department of Materials Science and Engineering, Irvine, Irvine, CA, 92697, United States

*Corresponding author email: patters3@uci.edu

Abstract

Polymerization-induced self-assembly (PISA) has emerged as a scalable one-pot technique to prepare block copolymer nanoparticles. Recently, we developed a PISA process that resulted in poly(L-lactide)-*b*-poly(ethylene glycol) block copolymer nanoparticles coined ring-opening polymerization-induced crystallization-driven self-assembly (ROPI-CDSA). The resulting nanorods demonstrated a strong propensity for aggregation, resulting in the formation of 2D sheets and 3D networks. Here, we report the synthesis of poly(*N,N*-dimethyl acrylamide)-*b*-poly(L)-lactide block copolymer nanoparticles by ROPI-CDSA utilizing a two-step, one-pot approach. A dual-functionalized photoiniferter was first used for controlled radical polymerization of the acrylamido-based monomer, and the resulting polymer served as a macroinitiator for organocatalyzed ring-opening polymerization to form the solvophobic polyester block. The resulting nanorods are highly stable and display anisotropy at higher molecular weights (>12k Da) and concentrations (>20% solids) than our previous report. This

development expands the chemical scope of ROPI-CDSA block copolymers and provides readily accessible nanorods made with biocompatible materials.

Introduction

Polymerization-induced self-assembly (PISA) has revolutionized the field of block copolymer self-assembly as it enables the reproducible and scalable production of nanoparticles.[1–3] In PISA, a macromolecular stabilizing block is chain extended with monomer that forms a solvophobic block. PISA can be conducted in solutions ranging from 10 to 50% solids wt in contrast to traditional methods, which typically yield nanoparticle solutions around 1% solids wt.[1,3,4] PISA has been developed for a wide range of polymerization techniques,[2,4–7] including for crystalline and semicrystalline polymers, termed polymerization-induced crystallization-driven self-assembly (PI-CDSA).[8] PI-CDSA has allowed for the scaled-up production of anisotropic nanostructures such as rods and lamellae.[8–12]

Recently, we developed PI-CDSA for the ring-opening polymerization (ROP) of semicrystalline polyesters, termed ring-opening polymerization-induced crystallization-driven self-assembly (ROPI-CDSA).[11–13] ROPI-CDSA is one of the earliest examples of PISA for ROP.[11–21] In this process, the poly(ethylene glycol) (PEG) macroinitiator was chain extended with L-lactide in toluene using various organocatalytic systems. The resulting poly(L-lactide)-block-pol(yethylene glycol) (PLLA-*b*-PEG) particle morphology varied from 1-D nanorods to 2-D lamellae, including 3-D stacked lamellae. However, the majority of nanoparticle dispersions displayed mixed morphologies, and we were not able to solely obtain well-defined nanorods.[11–13] Poly(*N,N*-dimethyl acrylamide)-*block*-poly(L)-lactide (PDMA-*b*-PLLA) is an excellent block copolymer (BCP) for controlled

crystallization-driven self-assembly of anisotropic nanorods and lamellae (CDSA), as demonstrated by O'Reilly et al.[22,23] In these studies, uniform morphologies were obtained. We reasoned that substitution of PEG for a polyacrylamido block such as PDMA would improve the uniformity and anisotropy of the assemblies resulting from ROPI-CDSA. Developing a PISA process for PDMA-*b*-PLLA would necessitate a controlled radical polymerization technique, followed by ROP. Hedrick et al. performed nitroxide-mediated polymerization of DMA using a nitroxide with a hydroxyl group followed by the ROP of L-lactide to synthesize PDMA-*b*-PLLA.[24,25] As far as we know, this is the sole example of PDMA-*b*-PLLA synthesis in a two-pot, two-step manner.[24–26]

Recently, Xia et al.[27] showed that photoiniferter polymerization and organocatalytic ROP could be performed stepwise or synchronously using a hydroxy-functionalized trithiocarbonate (TTC) dual-initiator for the one-pot production of polyacrylamido-*b*-polyether BCPs. Photoiniferters enable the polymerization of vinyl monomers with predictable molecular weights, low dispersity (*Đ*), and high end-group fidelity with the advantage of being performed at ambient conditions.[28–32] Organocatalytic ROP of lactides and lactones can be conducted using various catalysts and is typically performed under ambient conditions.[33,34] However, these ROPs are typically performed in solvents at monomer concentrations of around 1.0 M,[25,35] whereas the photoiniferter polymerization of polyacrylamides is carried out at higher monomer concentrations.[27]

Here, we describe a two-step, one-pot process to produce PDMA-*b*-PLLA based nanostructures. A TTC dual initiator-photoiniferter is first used to polymerize *N,N*-dimethyl acrylamide with the resultant macroinitiator being used for organocatalytic ROP of L-lactide in toluene to generate uniform BCP self-assemblies. Block lengths of the

solvophilic corona and solvophobic core were modified and studied by cryogenic transmission electron microscopy (cryoEM) to examine how block length impacts the resulting core and corona thickness.

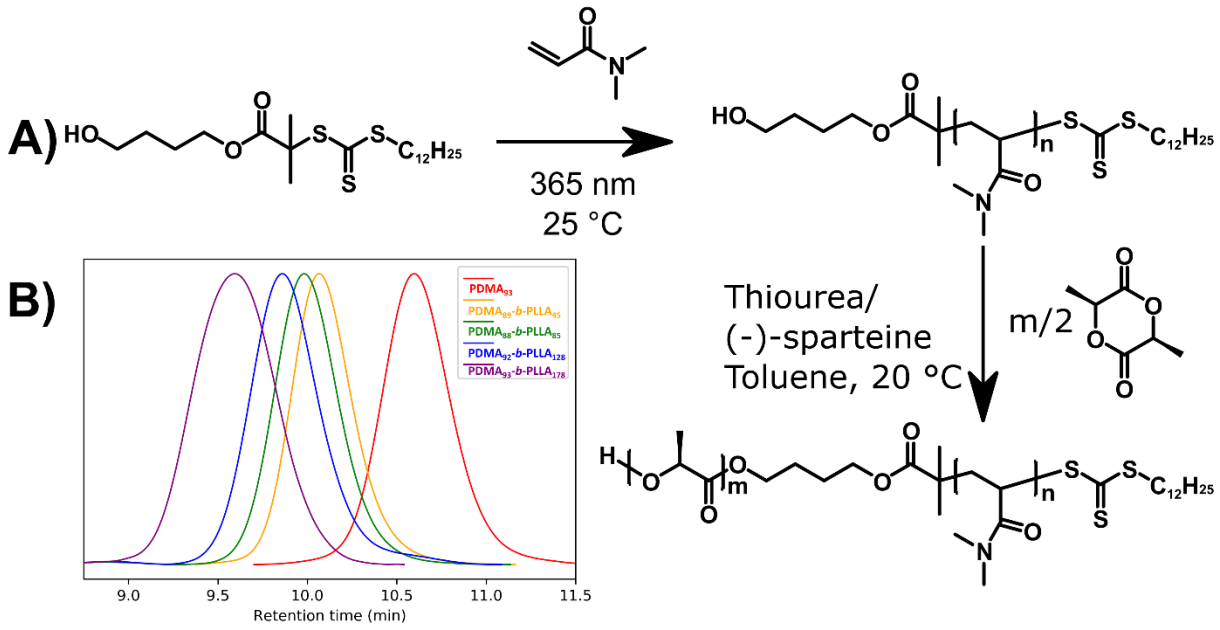

Figure 1: Synthesis of PDMA-b-PLLA. A) Scheme showing the photoiniferter polymerization of DMA (Step 1) followed by the polymerization of L-lactide to yield PDMA-b-PLLA (Step 2). The second step is carried out in toluene, which leads to self-assembly. B) Gel permeation chromatography in DMF showing the chain extension of the PDMA macroinitiator during the polymerization of LLA at varying degrees of polymerization.

Results and Discussion

As previously mentioned, photoiniferter polymerization of acrylamides and ROP of lactides and lactones are performed at different monomer concentrations, necessitating a sequential, one-pot approach. For the photoiniferter polymerization, we first synthesized

PDMA using previously optimized synthetic conditions.[27] Next, we developed and optimized the synthetic conditions for the second step of organocatalytic ROP. Initially, we used diazabicyclodecene (DBU), an excellent catalyst for the ROP of L-lactide, but the resulting PDMA-*b*-PLLA BCPs had dispersity values over 1.1 (Figure S1). Therefore, we switched to a milder and slower catalytic system based on thiourea (TU) and (-)-sparteine (Figure 1, Table 1).[35] Additionally, we reasoned that this slower reaction rate would lead to more control over self-assembly.[12] Keeping L-lactide concentration at 10% solids resulted in low dispersity (<1.1) while maintaining reasonable conversions (>66-95%) after four days of stirring at room temperature (~20 °C). A consequence of maintaining L-lactide concentration at 10% solids is that the total polymer concentration varies widely as target block lengths of the PDMA and PLLA blocks change. This variation leads to reactions targeting higher degrees of polymerization (DP) of PDMA being more concentrated. The target DP of both PDMA and PLLA was varied from 50-200 to produce a library of BCPs (Table S1 with select samples in Table 1). All polymers had low dispersity (<1.1) with shorter PDMA blocks giving higher conversion. Most of the resulting copolymer dispersions also became turbid, indicative of in-situ self-assembly.

Table 1: Synthetic parameters and results for select two-step, one-pot PDMA-*b*-PLLA synthesis.

Sample ID	Target DMA DP	DMA Conversion	Target LA DP	LA Conversion	Polymer Structure	$Đ$[b]	M_n (g/mol)	Polymer wt. %

	DP	sion (%)[a]	DP	sion (%)[a]				
1	100	92	150	85	PDMA$_{92}$-*b*-PLLA$_{128}$	1.06	18300	19.1
2	150	90	100	73	PDMA$_{135}$-*b*-PLLA$_{73}$	1.06	18600	30.6
3	150	95	150	71	PDMA$_{142}$-*b*-PLLA$_{107}$	1.07	21800	23.8
4	150	93	200	70	PDMA$_{139}$-*b*-PLLA$_{140}$	1.07	23900	20.3
5	200	90	100	74	PDMA$_{179}$-*b*-PLLA$_{74}$	1.07	23100	37.5

CryoEM was used to determine the morphology of the PDMA-*b*-PLLA dispersions (Figure 2). The nanoparticles were extracted into excess water from toluene to yield concentrations around 0.25-5 mg/mL.[11] The PLLA crystallinity serves as a kinetic trap at room temperature, allowing the morphology to be retained upon transfer to water.[11] CryoEM images show both the core and the corona blocks. While polymeric coronas are

often not visible in cryoEM, direct visualization has been demonstrated previously,[36] in particular with acrylamido-based amphiphilic homopolymers.[37]

All BCP dispersions consisted primarily of nanorods, with no appreciable lamellar nanostructures. Wide-angle X-ray scattering (WAXS) confirmed the semicrystalline nature of the PLLA blocks (Figure S2). BCP dispersions **2** and **5** were entirely nanorods, while **3** and **1** contained a few lamellar aggregates that appear to result from rod fusion, and **4** contained larger lamellar aggregates. BCP dispersions **2** and **5** varied corona block length with PDMA DPs of 135 and 179, respectively, and PLLA DPs of 73 and 74, respectively. Corona thickness, measured as the total thickness of the nanorods after subtracting the thickness of the core, was 27.1 ± 2.8 nm for **2** and 35.6 ± 2.6 nm for **5**. These results are expected, as core and corona thickness should increase with increasing DP of PLLA and PDMA, respectively.[38] This trend was also observed for BCP dispersions **3** and **1**, where the PDMA DPs were 142 and 92, respectively, and the PLLA DPs were 107 and 128, respectively (Figure 3, Table 2).

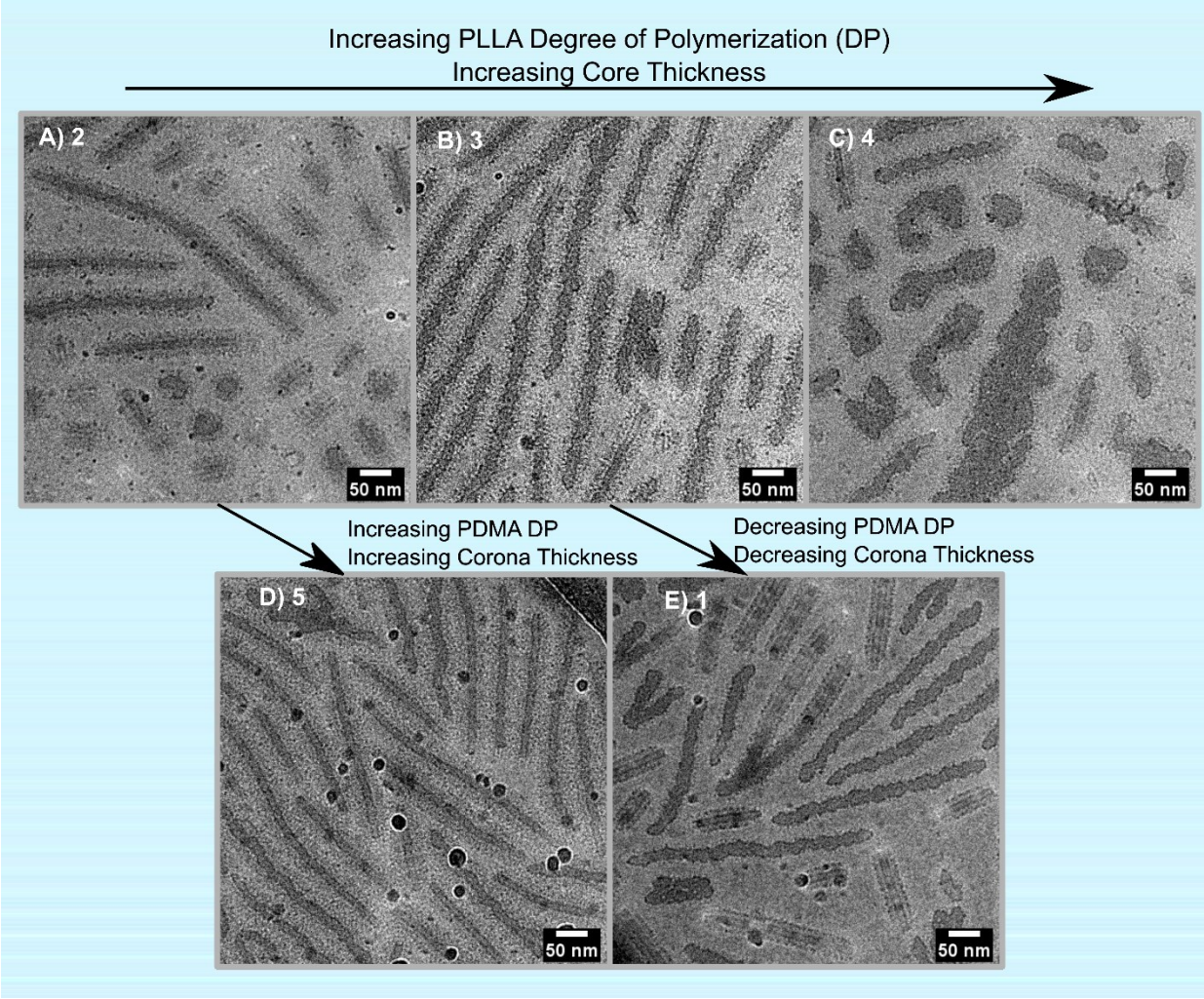

Figure 2: CryoEM images of select PDMA-b-PLLA BCPs. Images are labeled with the representative sample number (Table 1). Images **A-C** show the effect on core thickness and morphology with increasing PLLA chain length. Images **D-E** show the effect on corona thickness with changes in the PDMA chain length, with **D** having a longer PDMA chain than **A** with similar PLLA lengths and **E** having a shorter PDMA chain than **B** with similar PLLA lengths. Dark spheres present in these images are ice contamination, an artifact of cryoEM sample handling.

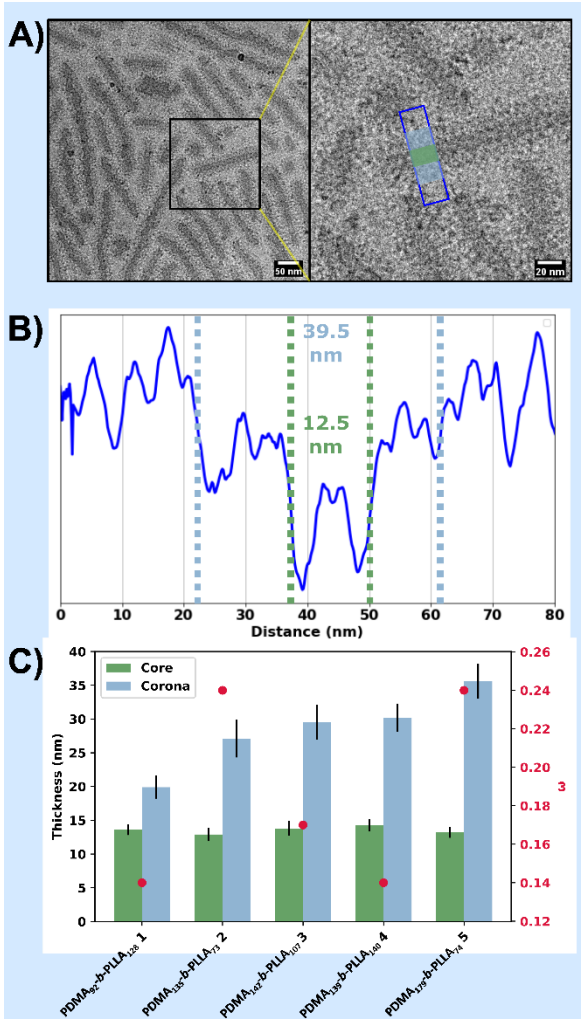

Figure 3: CryoEM core and corona nanorod measurements for PDMA-*b*-PLLA BCP dispersions. A) Representative cryoEM of **2** (left) with inset (right) with the line profile area in the blue box. B) Line profile of nanorod in A showing the measurement of the thickness of the core (green) and the total rod thickness (blue). Corona thickness is calculated by subtracting total thickness from the core thickness. C) Plot of core and corona thickness and the degree of polymer chain stretching (ω) for samples **1**-**5**.

Table 2: CryoEM core and corona nanorod measurements for PDMA-*b*-PLLA BCP dispersions. Results are graphically represented in Figure 3C.

Sample ID	Polymer Structure	Total thickness (nm)	Core thickness (nm)	ω*	Corona thickness (nm)

1	PDMA$_{92}$-*b*-PLLA$_{128}$	33.5 ± 1.5	13.6 ± 0.8	0.14	19.9 ± 1.7
2	PDMA$_{135}$-*b*-PLLA$_{73}$	40.0 ± 2.6	12.9 ± 1.0	0.24	27.1 ± 2.8
3	PDMA$_{142}$-*b*-PLLA$_{107}$	43.3 ± 2.4	13.8 ± 1.1	0.17	29.5 ± 2.6
4	PDMA$_{139}$-*b*-PLLA$_{140}$	44.5 ± 2.2	14.3 ± 0.9	0.14	30.2 ± 2.1
5	PDMA$_{179}$-*b*-PLLA$_{74}$	48.8 ± 2.5	13.2 ± 0.8	0.24	35.6 ± 2.6

*ω = degree of polymer chain stretching (core block only)

BCP dispersions **2**, **3**, and **4**, representing PDMA$_{135}$-*b*-PLLA$_n$ polymers with n (DP) = 73, 107, and 140, respectively, showed a clear trend in nanorod core thickness increasing with PLLA block length from 12.9 ± 1.0 nm core thickness in **2**, 13.8 ± 1.0 nm in **3**, and 14.3 ± 0.9 nm in **4** (Table 2). This series also shows an interesting morphology transition from nanorods with a uniform core thickness (**2**) to nanorods with a rough (jagged) core-corona interface (**3**) to a more complex mixture of nanorods and lamellae morphology (**4**). To better understand this transition, we calculate the degree of core polymer chain stretching (ω) as the ratio of the nanorod core radius (r) to the maximum theoretical length of the core polymer chain (L_{max}) (Eq. 1, Figure 3C, Table 2).[11,39]

$$\omega = \frac{r}{L_{max}} \quad (1)$$

Using an L_{max} of 3.69 Å * PLLA DP,[11] ω changes from 0.24 in **2** to 0.17 in **3** to 0.14 in **4**, indicating that the PLLA core is more highly foldedat higher PLLA DP, resulting in a reduced corona density. This reduction in density is also supported by the apparent reduction in corona contrast from **2** to **3** to **4**. As the corona density decreases, the growth mechanism may shift from unimer growth to a hybrid unimer growth/particle aggregation mechanism.[11] Additionally, **5**, with the same PLLA DP as **2**, also had an ω of 0.24 despite

a longer corona block. Therefore, ω may have stronger dependence on the PLLA DP than the molar ratio of PLLA to PDMA.

Conclusion

In conclusion, we demonstrate a new synthetic approach to well-defined polyacrylamido-*block*-polyester nanoparticles by leveraging a dual photoiniferter, ROPI-CDSA approach. The resulting nanoparticles of the PDMA-*b*-PLLA synthesis showed excellent anisotropy and uniformity when compared to the PLLA-*b*-PEG assemblies from our previous work. Lower PLLA DP nanorods are particularly anisotropic due to their higher corona densities compared to that of the than higher PLLA DP nanorods. This work represents a scalable technique for obtaining uniform nanorods made from biocompatible materials.

Experimental Section:

Materials: *N,N*-Dimethylacrylamide (DMA, Sigma Aldrich) was dried using calcium hydride and vacuum distilled and stored under 4 Å molecular sieves. 4-Hydroxybutyl 2-((dodecylthiocarbonothioyl)thio)-2-methylpropanoate was synthesized according to previous literature procedures.[27] L-Lactide (TCI) was recrystallized three times from toluene. Anhydrous toluene (99.8%), DBU, and (−)-sparteine were obtained from Sigma-Aldrich and stored under 4 Å molecular sieves. Benzoic acid (Fisher Chemical) was used without further purification. Thiourea (TU) derived from cyclohexylamine (Sigma-Aldrich) and 3,5-bis(trifluoromethyl)phenyl isothiocyanate (TCI) was synthesized following established literature procedures.[35] Chemicals were stored in a dry-N_2 atmosphere glovebox. Reactions were performed in a N_2 glovebox.

Synthetic Procedures: Photoiniferter polymerization of DMA (Step 1): DMA (208 mg, 2.1 mmol, target DP = 150) and 0.1 mL stock solution of 4-Hydroxybutyl 2-((dodecylthiocarbonothioyl)thio)-2-methylpropanoate in toluene (6.0 mg, 1.4 × 10-2 mmol) were charged to an 8-mL vial. The vial was sealed with a chemically inert screw cap and irradiated with UV light (365 nm, 3.5 mW cm^{-2}) for 8 h under stirring at room temperature (25 °C with light source).

Ring-opening polymerization of L-lactide (Step 2): L-Lactide (151 mg, 1.1 mmol, target DP = 150) was added to a solution of hydroxy functionalized PDMA from Step 1 (214 mg, 1.4 × 10-2 mmol mmol) and 10% mol TU (35 mg, 103 μmol) in 1.16 mL of toluene (10% L-lactide w/w). Next, 10% mol (−)-sparteine (24 μL, 103 μmol) was added. The solution was stirred for 4 days at 400 rpm at room temperature (20 °C) and subsequently quenched with 0.05 mL of saturated benzoic acid toluene solution.

Structural characterization: Proton nuclear magnetic resonance (^{1}H NMR) spectra were collected on a 500 MHz Bruker Avance spectrometer in $CDCl_3$ (Figure S3). Chemical shifts are given in ppm, calibrated from residual $CHCl_3$. Conversion was calculated for DMA polymerization by comparing the monomer peaks (5.7, 6.3, 6.6) ppm to the end group 0.95 ppm. Conversion was calculated for L-lactide polymerization by comparing the peak area of the PLLA peak at 5.16 ppm to the L-lactide monomer peak at 5.03 ppm. Size exclusion chromatography (SEC) was performed in DMF using an Agilent 1100 chromatograph equipped with RID detector and a PL gel 5 μm 300 × 7.5 mm mixed column at 40 °C. Samples were calibrated against polystyrene standards.

Wide-angle X-ray Scattering (WAXS) were measured using lyophilized polymer samples on a Rigaku Smart lab X-ray diffractometer in Bragg–Brentano diffraction mode utilizing

X-rays generated at 40 kV and 44 mA with Cu Kα irradiation (step size 0.02°, speed 1.0, IS 0.5°, RS1 4.0°, RS2 13 mm).

Cryogenic-transmission electron microscopy (cryoEM) samples were prepared on Quantifoil grids (R 2/2 40 Mesh, Electron Microscopy Sciences) from original samples that were extracted into excess water from toluene giving final concentrations of ≈ 0.1 μg/mL. Extraction was performed by diluting a small volume of the reaction mixture (~5–10 μL) into an uncapped vial of excess water (~2 mL) and vortexing the solution briefly followed by gentle sonication for 5 minutes. The vials were capped after several hours, allowing the toluene to evaporate.[13] Vitrification was carried out by an Automatic Plunge Freezer ME GP2 (Leica Microsystems) with 3 μL of sample. Grid preparation was performed at >95% humidity and the grids were blotted for 3 s prior to plunging into liquid nitrogen. CryoEM samples were then placed on a Gatan cryoEM holder and imaged on a JEOL 2100F transmission electron microscope using a Schottky type field emission gun operating at 200 keV. Images were recorded using SerialEM software in low dose imaging mode with a Gatan OneView CMOS camera at 4k × 4k resolution.

Acknowledgements: This material is primarily funded by the National Science Foundation (NSF) grant DMR-22238834. Secondary support by DMR-1904631. The authors acknowledge the use of facilities and instrumentation at the UC Irvine Materials Research Institute (IMRI) supported in part by the NSF Materials Research Science and Engineering Center program through the UC Irvine Center for Complex and Active Materials (DMR-2011967).

References:

(1) Canning, S. L.; Smith, G. N.; Armes, S. P. A Critical Appraisal of RAFT-Mediated Polymerization-Induced Self-Assembly. *Macromolecules* **2016**, *49* (6), 1985–2001. https://doi.org/10.1021/acs.macromol.5b02602.

(2) Cao, J.; Tan, Y.; Chen, Y.; Zhang, L.; Tan, J. Expanding the Scope of Polymerization-Induced Self-Assembly: Recent Advances and New Horizons. *Macromol. Rapid Commun.* **2021**, *42* (23), 2100498. https://doi.org/10.1002/marc.202100498.

(3) Phan, H.; Cossutta, M.; Houppe, C.; Le Cœur, C.; Prevost, S.; Cascone, I.; Courty, J.; Penelle, J.; Couturaud, B. Polymerization-Induced Self-Assembly (PISA) for in Situ Drug Encapsulation or Drug Conjugation in Cancer Application. *J. Colloid Interface Sci.* **2022**, *618*, 173–184. https://doi.org/10.1016/j.jcis.2022.03.044.

(4) Liu, C.; Hong, C.-Y.; Pan, C.-Y. Polymerization Techniques in Polymerization-Induced Self-Assembly (PISA). *Polym. Chem.* **2020**, *11* (22), 3673–3689. https://doi.org/10.1039/D0PY00455C.

(5) Zhao, Z.; Lei, S.; Zeng, M.; Huo, M. Recent Progress in Polymerization-Induced Self-Assembly: From the Perspective of Driving Forces. *Aggregate* **2024**, *5* (1), e418. https://doi.org/10.1002/agt2.418.

(6) Zhu, C.; Nicolas, J. (Bio)Degradable and Biocompatible Nano-Objects from Polymerization-Induced and Crystallization-Driven Self-Assembly. *Biomacromolecules* **2022**, *23* (8), 3043–3080. https://doi.org/10.1021/acs.biomac.2c00230.

(7) Zhang, S.; Li, R.; An, Z. Degradable Block Copolymer Nanoparticles Synthesized by Polymerization-Induced Self-Assembly. *Angew. Chem.* **2024**, *136* (12), e202315849. https://doi.org/10.1002/ange.202315849.

(8) Boott, C. E.; Gwyther, J.; Harniman, R. L.; Hayward, D. W.; Manners, I. Scalable and Uniform 1D Nanoparticles by Synchronous Polymerization, Crystallization and Self-Assembly. *Nat. Chem.* **2017**, *9*, 785. https://doi.org/10.1038/nchem.2721.

(9) Sha, Y.; Rahman, M. A.; Zhu, T.; Cha, Y.; McAlister, C. W.; Tang, C. ROMPI-CDSA: Ring-Opening Metathesis Polymerization-Induced Crystallization-Driven Self-Assembly of Metallo-Block Copolymers. *Chem. Sci.* **2019**, *10* (42), 9782–9787. https://doi.org/10.1039/C9SC03056E.

(10) Hwang, S.-H.; Kang, S.-Y.; Yang, S.; Lee, J.; Choi, T.-L. Synchronous Preparation of Length-Controllable 1D Nanoparticles via Crystallization-Driven In Situ Nanoparticlization of Conjugated Polymers. *J. Am. Chem. Soc.* **2022**, *144* (13), 5921–5929. https://doi.org/10.1021/jacs.1c13385.

(11) Hurst, P. J.; Rakowski, A. M.; Patterson, J. P. Ring-Opening Polymerization-Induced Crystallization-Driven Self-Assembly of Poly-L-Lactide-Block-Polyethylene Glycol Block Copolymers (ROPI-CDSA). *Nat. Commun.* **2020**, *11* (1), 4690. https://doi.org/10.1038/s41467-020-18460-2.

(12) Hurst, P. J.; Graham, A. A.; Patterson, J. P. Gaining Structural Control by Modification of Polymerization Rate in Ring-Opening Polymerization-Induced Crystallization-Driven Self-Assembly. *ACS Polym. Au* **2022**, *2* (6), 501–509. https://doi.org/10.1021/acspolymersau.2c00027.

(13) Hurst, P. J.; Gassaway, K. J.; Abouchaleh, M. F.; Idris, N. S.; Jones, C. R.; Dicksion, C. A.; Nowick, J. S.; Patterson, J. P. Drug Catalyzed Polymerization Yields

One Pot Nanomedicines. *RSC Appl. Polym.* **2024**. https://doi.org/10.1039/D3LP00135K.
(14) Grazon, C.; Salas-Ambrosio, P.; Ibarboure, E.; Buol, A.; Garanger, E.; Grinstaff, M. W.; Lecommandoux, S.; Bonduelle, C. Aqueous Ring-Opening Polymerization-Induced Self-Assembly (ROPISA) of N-Carboxyanhydrides. *Angew. Chem. Int. Ed.* **2020**, *59* (2), 622–626. https://doi.org/10.1002/anie.201912028.
(15) Grazon, C.; Salas-Ambrosio, P.; Antoine, S.; Ibarboure, E.; Sandre, O.; J. Clulow, A.; J. Boyd, B.; W. Grinstaff, M.; Lecommandoux, S.; Bonduelle, C. Aqueous ROPISA of α-Amino Acid N -Carboxyanhydrides: Polypeptide Block Secondary Structure Controls Nanoparticle Shape Anisotropy. *Polym. Chem.* **2021**, *12* (43), 6242–6251. https://doi.org/10.1039/D1PY00995H.
(16) Shi, Q.; Chen, Y.; Yang, J.; Yang, J. Ring-Opening Polymerization-Induced Self-Assembly (ROPISA) of Salicylic Acid o -Carboxyanhydride. *Chem. Commun.* **2021**, *57* (86), 11390–11393. https://doi.org/10.1039/D1CC04630F.
(17) Yao, S.; Yang, J.; Yang, J. ROPISA of Salicylic Acid O -Carboxyanhydride: Fast Polymerization Followed by in Situ Kinetics-Driven Self-Assembly. *Polym. Chem.* **2023**, *14* (30), 3493–3500. https://doi.org/10.1039/D3PY00550J.
(18) Shen, D.; Shi, B.; Zhou, P.; Li, D.; Wang, G. Temperature-Dependent Ring-Opening Polymerization-Induced Self-Assembly Using Crystallizable Polylactones as Core-Forming Blocks. *Macromolecules* **2023**, *56* (13), 4814–4822. https://doi.org/10.1021/acs.macromol.3c00681.
(19) Xi Huang, S.; Hao Wang, Z.; Lin, M.; Hui Fu, X.; Sun, J. One-Pot Preparation of Polypeptide Nanogels in Aqueous Solution via Ring-Opening Polymerization-Induced Nano-Gelation. *Polym. Chem.* **2023**, *14* (15), 1801–1808. https://doi.org/10.1039/D3PY00206C.
(20) Jiang, J.; Zhang, X.; Fan, Z.; Du, J. Ring-Opening Polymerization of N-Carboxyanhydride-Induced Self-Assembly for Fabricating Biodegradable Polymer Vesicles. *ACS Macro Lett.* **2019**, *8* (10), 1216–1221. https://doi.org/10.1021/acsmacrolett.9b00606.
(21) Ellis, C. E.; Garcia-Hernandez, J. D.; Manners, I. Scalable and Uniform Length-Tunable Biodegradable Block Copolymer Nanofibers with a Polycarbonate Core via Living Polymerization-Induced Crystallization-Driven Self-Assembly. *J. Am. Chem. Soc.* **2022**, *144* (44), 20525–20538. https://doi.org/10.1021/jacs.2c09715.
(22) Inam, M.; Cambridge, G.; Pitto-Barry, A.; Laker, Z. P. L.; Wilson, N. R.; Mathers, R. T.; Dove, A. P.; O'Reilly, R. K. 1D vs. 2D Shape Selectivity in the Crystallization-Driven Self-Assembly of Polylactide Block Copolymers. *Chem. Sci.* **2017**, *8* (6), 4223–4230. https://doi.org/10.1039/C7SC00641A.
(23) Yu, W.; Inam, M.; Jones, J. R.; Dove, A. P.; O'Reilly, R. K. Understanding the CDSA of Poly(Lactide) Containing Triblock Copolymers. *Polym. Chem.* **2017**, *8* (36), 5504–5512. https://doi.org/10.1039/C7PY01056G.
(24) Kim, S. H.; Nederberg, F.; Zhang, L.; Wade, C. G.; Waymouth, R. M.; Hedrick, J. L. Hierarchical Assembly of Nanostructured Organosilicate Networks via Stereocomplexation of Block Copolymers. *Nano Lett.* **2008**, *8* (1), 294–301. https://doi.org/10.1021/nl0726813.
(25) Lohmeijer, B. G. G.; Pratt, R. C.; Leibfarth, F.; Logan, J. W.; Long, D. A.; Dove, A. P.; Nederberg, F.; Choi, J.; Wade, C.; Waymouth, R. M.; Hedrick, J. L. Guanidine

and Amidine Organocatalysts for Ring-Opening Polymerization of Cyclic Esters. *Macromolecules* **2006**, *39* (25), 8574–8583. https://doi.org/10.1021/ma0619381.
(26) Yildirim, I.; Weber, C.; Schubert, U. S. Old Meets New: Combination of PLA and RDRP to Obtain Sophisticated Macromolecular Architectures. *Prog. Polym. Sci.* **2018**, *76*, 111–150. https://doi.org/10.1016/j.progpolymsci.2017.07.010.
(27) Xia, Y.; Scheutz, G. M.; Easterling, C. P.; Zhao, J.; Sumerlin, B. S. Hybrid Block Copolymer Synthesis by Merging Photoiniferter and Organocatalytic Ring-Opening Polymerizations. *Angew. Chem.* **2021**, *133* (34), 18685–18689. https://doi.org/10.1002/ange.202106418.
(28) Hartlieb, M. Photo-Iniferter RAFT Polymerization. *Macromol. Rapid Commun.* **2022**, *43* (1), 2100514. https://doi.org/10.1002/marc.202100514.
(29) Carmean, R. N.; Sims, M. B.; Figg, C. A.; Hurst, P. J.; Patterson, J. P.; Sumerlin, B. S. Ultrahigh Molecular Weight Hydrophobic Acrylic and Styrenic Polymers through Organic-Phase Photoiniferter-Mediated Polymerization. *ACS Macro Lett.* **2020**, *9* (4), 613–618. https://doi.org/10.1021/acsmacrolett.0c00203.
(30) Davidson, C. L. G. I.; Lott, M. E.; Trachsel, L.; Wong, A. J.; Olson, R. A.; Pedro, D. I.; Sawyer, W. G.; Sumerlin, B. S. Inverse Miniemulsion Enables the Continuous-Flow Synthesis of Controlled Ultra-High Molecular Weight Polymers. *ACS Macro Lett.* **2023**, 1224–1230. https://doi.org/10.1021/acsmacrolett.3c00431.
(31) Hughes, R. W.; Lott, M. E.; Bowman, J. I.; Sumerlin, B. S. Excitation Dependence in Photoiniferter Polymerization. *ACS Macro Lett.* **2023**, *12* (1), 14–19. https://doi.org/10.1021/acsmacrolett.2c00683.
(32) Olson, R. A.; Lott, M. E.; Garrison, J. B.; Davidson, C. L. G. I.; Trachsel, L.; Pedro, D. I.; Sawyer, W. G.; Sumerlin, B. S. Inverse Miniemulsion Photoiniferter Polymerization for the Synthesis of Ultrahigh Molecular Weight Polymers. *Macromolecules* **2022**, *55* (19), 8451–8460. https://doi.org/10.1021/acs.macromol.2c01239.
(33) Kamber, N. E.; Jeong, W.; Waymouth, R. M.; Pratt, R. C.; Lohmeijer, B. G. G.; Hedrick, J. L. Organocatalytic Ring-Opening Polymerization. *Chem. Rev.* **2007**, *107* (12), 5813–5840. https://doi.org/10.1021/cr068415b.
(34) Thomas, C.; Bibal, B. Hydrogen-Bonding Organocatalysts for Ring-Opening Polymerization. *Green Chem.* **2014**, *16* (4), 1687–1699. https://doi.org/10.1039/C3GC41806E.
(35) Pratt, R. C.; Lohmeijer, B. G. G.; Long, D. A.; Lundberg, P. N. P.; Dove, A. P.; Li, H.; Wade, C. G.; Waymouth, R. M.; Hedrick, J. L. Exploration, Optimization, and Application of Supramolecular Thiourea−Amine Catalysts for the Synthesis of Lactide (Co)Polymers. *Macromolecules* **2006**, *39* (23), 7863–7871. https://doi.org/10.1021/ma061607o.
(36) Danino, D.; Talmon, Y.; Zana, R. Cryo-TEM of Thread-like Micelles: On-the-Grid Microstructural Transformations Induced during Specimen Preparation. *Colloids Surf. Physicochem. Eng. Asp.* **2000**, *169* (1), 67–73. https://doi.org/10.1016/S0927-7757(00)00418-0.
(37) Patterson, J. P.; Kelley, E. G.; Murphy, R. P.; Moughton, A. O.; Robin, M. P.; Lu, A.; Colombani, O.; Chassenieux, C.; Cheung, D.; Sullivan, M. O.; Epps, T. H. I.; O'Reilly, R. K. Structural Characterization of Amphiphilic Homopolymer Micelles

Using Light Scattering, SANS, and Cryo-TEM. *Macromolecules* **2013**, *46* (15), 6319–6325. https://doi.org/10.1021/ma4007544.
(38) Mai, Y.; Eisenberg, A. Self-Assembly of Block Copolymers. *Chem. Soc. Rev.* **2012**, *41* (18), 5969–5985. https://doi.org/10.1039/C2CS35115C.
(39) Patterson, J. P.; Robin, M. P.; Chassenieux, C.; Colombani, O.; O'Reilly, R. K. The Analysis of Solution Self-Assembled Polymeric Nanomaterials. *Chem. Soc. Rev.* **2014**, *43* (8), 2412–2425. https://doi.org/10.1039/C3CS60454C.